https://doi.org/10.5194/egusphere-2026-981
Preprint. Discussion started: 16 March 2026

Process-based evaluation of green roof models for assessment of heat mitigation efficacy in WRF (v4.3.1) and EnergyPlus (v8.6.0)

Maria Martinez Mendoza[1], Alireza Saeedi[2], James A. Voogt[1], E. Scott Krayenhoff[2]

[1]Department of Geography and Environment, The University of Western Ontario, London, Ontario, Canada.
[2]School of Environmental Sciences, University of Guelph, Guelph, Ontario, Canada.

Correspondence to: Maria Martinez Mendoza (mmart376@uwo.ca)

Abstract. Green roofs mitigate urban heat, but to fully assess their impact, green roof models must be integrated into urban climate models, where they provide critical surface boundary conditions. Ensuring their reliability requires evaluation, yet such efforts remain limited in the literature. This study addresses that gap by evaluating two configurations of EcoRoof, the green roof module from EnergyPlus (ER_o for the original version of the model, and ER_m for a modified version), and a multilayer green roof parametrization for WRF (WRF-MLGR) (Heusinger et al., 2018; Sailor, 2008; Zonato et al., 2021). These models were tested against field observations from a monitored green roof in London, Ontario, focusing on latent heat flux (Q_e), surface temperature (T_{surf}), storage heat flux (Q_g) and soil water content (SWC). Model performance varied by variable. The two EcoRoof versions showed similar performance, with mean RMSE across study periods of approximately 56-60 W m^{-2} for Q_e, 3-4 °C for T_{surf}, 22 W m^{-2} for Q_g, and 0.03 m^3 m^{-3} for SWC. Performance for Q_e was comparable across models; however, WRF-MLGR exhibited much larger errors for Q_g (with mean RMSE exceeding 100 W m^{-2}) and SWC (0.06 m^3 m^{-3}), along with higher T_{surf} deviations (~5 °C). Overall, EcoRoof provided a more consistent representation of the daytime energy balance, whereas WRF-MLGR showed structural biases in surface heating. These findings highlight the importance of process-level evaluation for urban climate applications and underscore the need for continued model development to address the structural limitations in green roof parametrizations.

https://doi.org/10.5194/egusphere-2026-981
Preprint. Discussion started: 16 March 2026

1. Introduction

Green roofs have emerged as a promising technology to enhance urban resilience. They consist of vegetation on the rooftops of buildings and offer numerous environmental benefits, such as mitigating urban heat, reducing building energy use, reducing stormwater runoff and contributing to biodiversity and urban livability (Berardi et al., 2014; Oberndorfer et al., 2007; Shafique et al., 2018). Their ability to influence the surface energy balance makes them particularly valuable as an urban heat adaptation strategy. Vegetation and moist growing media redirect energy into the latent heat flux through evapotranspiration, thereby reducing sensible heat flux to the atmosphere, while the soil's thermal mass dampens diurnal temperature extremes (Li et al., 2014) and acts as a layer of insulation providing year round benefit to the host building.

To capture these effects at the city scale, green roofs must be incorporated into urban canopy models, where reliable parameterizations can provide critical surface boundary conditions for simulations of urban climate adaptation. Rigorous evaluation of their underlying energy-balance schemes is essential for reliable integration into city-scale applications (Krayenhoff et al. 2021). While many studies include green roofs as an adaptation measure (Berardi, 2016; He et al., 2020; Heusinger and Weber, 2017; Jaffal et al., 2012; Kim et al., 2024; Krayenhoff et al., 2003; Liu and Minor, 2005; Martens et al., 2008; Seo et al., 2023; Silva et al., 2016; Zheng et al., 2022), most rely on parameterizations without thoroughly assessing model performance. Furthermore, when evaluation is performed, it usually focuses on outcome variables such as surface or soil temperature. Krayenhoff et al. (2021) emphasize that evaluating surface energy fluxes (i.e., the physical processes) offers a more robust insight and is essential to ensure accurate and dependable results.

As part of ongoing efforts to improve green-roof representation in urban canopy models (Siddiqui et al., 2022), we evaluate two existing green-roof models: EcoRoof included in EnergyPlus (Sailor, 2008) and a green roof model coupled in the multi-layer urban canopy model BEP-BEM (Martilli et al. 2002) within the Weather and Research Forecasting model (WRF), hereafter referred to as WRF-MLGR (Zonato et al. 2021). These models were selected based on their availability, exportability, and potential integration into the GEM-TEB urban climate modelling framework. They represent contrasting levels of structural complexity and are embedded within widely used

https://doi.org/10.5194/egusphere-2026-981
Preprint. Discussion started: 16 March 2026

building and atmospheric modelling systems, making them strong candidates for comparative assessment.

Despite their widespread use, both models have rarely been subject to comprehensive evaluation. For EcoRoof, most applications emphasize thermal behavior or energy savings without model evaluation (e.g. Cascone et al. 2018; Zheng & Weng 2020; Costanzo et al. 2016). Studies that do include some form of evaluation, such as Silva et al. (2016) and Karachaliou et al. (2016), do not explicitly assess surface energy fluxes. Similarly, WRF-MLGR was first introduced by Zonato et al. (2021) within the WRF-BEP-BEM framework (Martilli et al., 2002; Salamanca et al., 2010), and its implementation rather than evaluation was emphasized. Applications of other WRF configurations (e.g. Kalogeri et al. 2023; and Imran et al. 2018) follow the same pattern of focusing on implementation rather than evaluation, and while some efforts at evaluation exist (e.g. Khan et al. 2023; Sun et al. 2016), these remain limited in scope.

Taken together, these examples highlight a common trend in literature: while these models are widely applied to estimate cooling potential, energy performance or inform design and policy decisions, their predictive accuracy is rarely scrutinized. This underscores the need for systematic evaluation of green roof models. To address this gap, we evaluate EcoRoof and WRF-MLGR against observations from a green roof test array. Specifically, we ask: (a) how well does each model reproduce fluxes (Q_e, Q_g) and T_{surf} during multi-month periods? (b) How does model performance change across different moisture regimes and radiative forcing conditions? and (c) how accurately do they simulate soil water content dynamics during and after precipitation events?

2. Methods

2.1 Site and experimental setup

The study site for this research is a green roof located on the rooftop of the Talbot College building, at Western University, London, Ontario, Canada. The green roof plot is composed of individual modules placed side by side, with dimensions of 0.3 m x 0.3 m and depths of 0.10 m and 0.15 m. The green roof does not completely cover the roof area; Fig. 1 shows a photograph of the green roof setting. It has three different types of vegetation: *Sedum spurium, Aquilegia canadensis,* and *Sporobolus heterolepis*.

https://doi.org/10.5194/egusphere-2026-981
Preprint. Discussion started: 16 March 2026

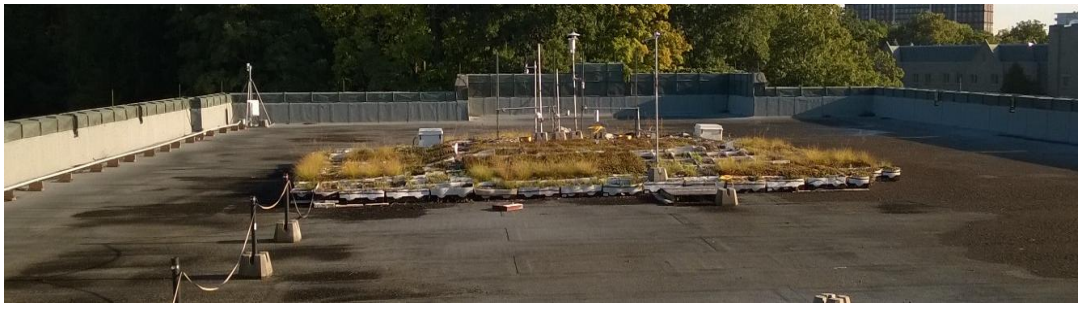

Figure 1: The green roof test array on Talbot College at Western University. Photo credit: J. Voogt

For this study, the observational data comes from a central array within the green roof which is elevated from the roof surface to allow the installation of lysimeters. The array consists of modules planted exclusively with *Sedum spurium.* The growing media was previously characterized by Perelli (2014) and was constructed as a homogeneous 0.15 m layer, with no intentional vertical differentiation in material composition. For analysis purposes, however, the substrate was treated analytically as a 2.5 cm surface layer and a 12.5 cm subsurface layer, reflecting sensor placement and root distribution rather than distinct physical layers within the growing medium.

2.2 Data collection and observed variables

This research uses observational data from the summer and fall seasons of 2014, collected from July 1st to October 31st, 2014. Details about the measured variables and instrumentation used can be found in Sect. S1 of the supplementary materials and on Kurukulaarachchi (2017). Energy-balance components and microclimate variables were sampled at 1-second intervals and subsequently averaged and stored at 5-minute resolution, lysimeters, rain gauges and drainage units were averaged (or totaled, as appropriate) over 1-minute intervals. A conceptual diagram of the green roof instrumentation set up is shown in Fig. 2.

https://doi.org/10.5194/egusphere-2026-981
Preprint. Discussion started: 16 March 2026

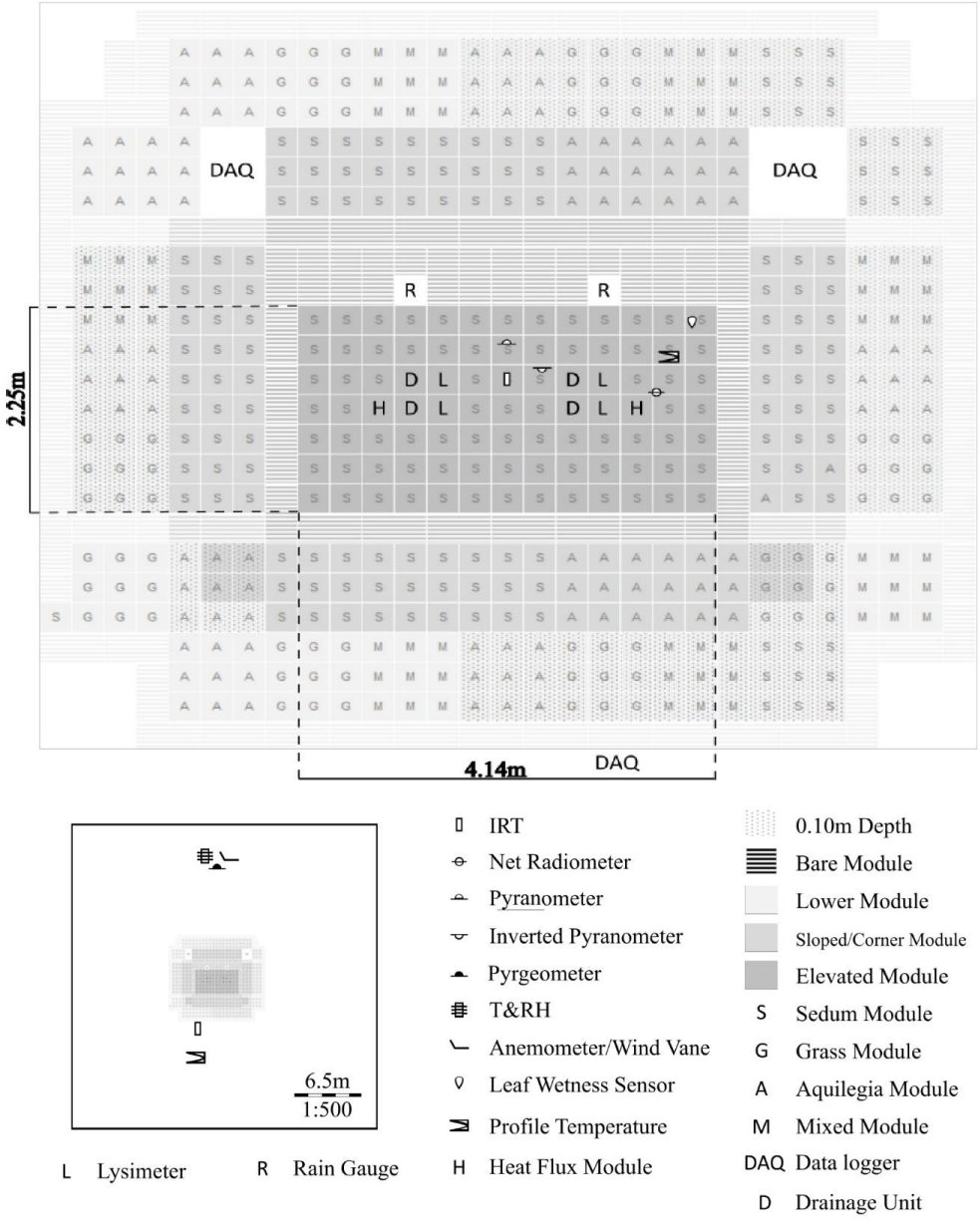

Figure 2: Green roof conceptual diagram (Kurukulaarachchi, 2017)

2.3 Selection of study periods and evaluation criteria

2.3.1 Selection of analysis periods

https://doi.org/10.5194/egusphere-2026-981
Preprint. Discussion started: 16 March 2026

To evaluate model performance, two analysis periods of 62 days were selected, each encompassing multiple precipitation events interspersed with drying intervals. Period selection was guided by a monthly stratification of the dataset, for which summary statistics (mean, standard deviation, and 25th, 50th, and 75th percentiles) were computed for net radiation, air temperature, vapor pressure deficit (VPD), and wind speed. Based on similarities in these environmental characteristics, July–August was grouped as 'summer' and September–October as 'fall'. These labels are used only for descriptive convenience and do not correspond to full meteorological seasons.

Two additional subsets were defined to isolate model performance under contrasting environmental conditions: dry versus rainy days and low versus high net radiation (Q^*). For the moisture-based classification, a daily rainfall threshold of > 5 mm was used to identify rainy days, while dry days were defined as having < 0.2 mm of rainfall on the target day and during the preceding two days. This classification yielded 15 rainy days in summer and 11 in fall, and 13 dry days in summer and 14 in fall.

For the radiation-based classification, high- and low-net radiation days were identified using percentile thresholds: days below the 25th percentile of daytime mean net radiation were classified as low-net radiation conditions, and days above the 75th percentile were classified as high-net radiation conditions. This procedure resulted in 31 low-net radiation days and 31 high-net radiation days across the analysis periods.

2.3.2 Evaluation criteria and data exclusions

Although the model simulates energy balance continuously, the focus of the evaluation is not on the accuracy of fluxes during precipitation itself, but rather on how well the model responds to rainfall inputs over time. To isolate this response, time steps with active precipitation (rainfall > 0.2 mm) were excluded at the analysis stage. This approach is consistent with the study objectives, as Q_e cannot be reliably estimated from lysimeters measurements during rainfall and moreover, evapotranspiration is minimal under these conditions due to high humidity and reduced vapor pressure gradients.

The evaluation was restricted to daytime conditions ($Q^* > 0$), when surface energy exchanges are dominated by radiative forcing and turbulent fluxes are most pronounced. In addition, time steps

https://doi.org/10.5194/egusphere-2026-981
Preprint. Discussion started: 16 March 2026

affected by instrument malfunction, calibration activities, or missing data were removed. All exclusions were applied only to the observed and modeled outputs used for evaluation; the simulations themselves were performed using the complete forcing datasets.

2.4 Derivation of observed energy balance

2.4.1 Energy balance framework and assumptions

The experimental green roof used in this study occupies only a portion of the roof surface (Fig. 1), surrounded by conventional roofing material, introducing potential for advective effects, as thermal gradients between the vegetated and bare roof surfaces may influence heat exchange. Kurukulaarachchi (2017) analyzed selected drying periods from 2014 and found that only 2.8% of the data showed possible signs of advection, with strong evidence present in just 1.2% of the cases. Advection in that study was identified under specific conditions—such as temperature inversions, wind directions associated with a large fetch across the bare roof surface, and large temperature differences between the green roof and surrounding surfaces—indicating the movement of warm, dry air across the vegetated modules.

Based on these findings, advective influences are expected to be minimal in the present dataset. Accordingly, the observational surface energy balance is formulated under the assumption of negligible horizontal energy fluxes, and is expressed as:

$$Q^* = Q_e + Q_h + Q_g \quad (1)$$

Before calculating observed Q_e and Q_g, the raw data underwent processing steps to ensure physical consistency and compatibility among variables. These steps included computing lysimeter weight changes, converting precipitation and drainage data into equivalent depths, deriving soil water content from lysimeter measurements, and estimating a soil heat capacity that accounts for changes in moisture. Observed Q_e was taken as the average of the two lysimeter-derived (northeast and southeast) estimates, whereas Q_g was derived from one module only (west module) due to extensive missing data in the other module. In addition, the radiative measurement of T_{surf} was corrected using an emissivity of 0.96 (Kurukulaarachchi, 2017), and the measured incident longwave radiation to represent kinetic temperature. Detailed derivations and processing steps for all variables are provided in Sect. S2 of the supplementary materials.

https://doi.org/10.5194/egusphere-2026-981
Preprint. Discussion started: 16 March 2026

2.5 Green Roof Energy Balance Models

2.5.1 Comparison of Model Approaches

The models to be compared are stand-alone versions of ER—an original version of the model, as found withing EnergyPlus v8.6.0 (Sailor, 2008), and a modified configuration following Heusinger et al. (2018)—and a stand-alone version of the green roof parametrization embedded in WRF v.4.3.1 (Zonato et al., 2021). Table 1 provides an overview of each model.

Table 1: Green roof model overview.

Characteristic	Model		
	ER_o (Sailor, 2008)	**ER_m Heusinger et al. (2018)**	**WRF-MLGR (Zonato et al., 2021)**
Dimensionality	One dimension (vertical).	One dimension (vertical).	One dimension (vertical).
Number of Layers	Two soil layers (a surface layer and a subsurface layer).	Two soil layers (a surface layer and a subsurface layer).	Ten layers (four corresponding to the built roof below six corresponding to the green roof soil).
Energy balance calculation	Separate assessment of energy balance for the foliage layer and for the soil surface.	Separate assessment of energy balance for the foliage layer and for the soil surface.	Lumped energy processes for foliage and soil surface with no explicit separation of canopy.
Radiative exchange	Accounts for long-wave and short-wave radiative exchange between plant canopy and soil.	Accounts for long-wave and short-wave radiative exchange between plant canopy and soil.	Calculates net radiation but does not detail intra-canopy or canopy-soil radiative exchanges.

https://doi.org/10.5194/egusphere-2026-981
Preprint. Discussion started: 16 March 2026

Convective heat transfer	Two-layer resistance-based model with explicit canopy air space	Two-layer resistance-based model with explicit canopy air space	Bulk aerodynamic method without soil-vegetation flux partitioning.
Evapotranspiration	Accounts for soil evaporation and plant transpiration, with stomatal resistance being influenced by environmental factors.	Accounts for soil evaporation, plant transpiration (influenced by environmental factors), and evaporation of intercepted rainfall.	Includes only plant transpiration influenced by environmental conditions; no soil evaporation.
Heat conduction and storage	Fourier's law.	Fourier's law.	Fourier's law.
Soil thermal properties	Moisture-dependent.	Moisture-dependent.	Moisture-dependent.
Runoff/drainage	Occurs when rainfall exceeds a fixed infiltration threshold and when layers exceed saturation; drainage from the subsurface layer conductivity-based.	Includes canopy interception with drip to the soil and replaces fixed infiltration threshold with moisture-dependent surface runoff calculation.	Drainage occurs from the bottom layer using a moisture-dependent conductivity function. Does not include explicit surface runoff or canopy interception.

2.5.2 Model set up

In addition to input parameters, which need to be specified in the program, the models require an input file with atmospheric forcing data, which is common to both models. It consists of time series measurements of eight variables: incoming solar radiation, incoming longwave radiation, wind speed, air temperature, humidity, precipitation, air pressure and irrigation. Most variables were directly measured on site, except air pressure, which was retrieved from London A weather station (WMO ID: 71623), located at London International Airport. The models also require certain

https://doi.org/10.5194/egusphere-2026-981
Preprint. Discussion started: 16 March 2026

variables to be initialized, the specific variables vary according to the model and are specified in Sect. S5 of the supplementary materials, along with the input parameters required by the models. The models are initialized (forcing file starts) at 03:00 LT on the first day of the period and end at 23:00 LT on the last day of the period. The timesteps are 5 minutes long and the values used for the initialization correspond to the value at the 03:00 time step for all variables except albedo, which is an average.

2.6 Evaluation metrics

For the model evaluation a quantitative analysis was performed to compare modeled and observed values. The statistical metrics calculated are Mean Absolute Error (MAE), Mean Bias Error (MBE) and Root Mean Square Error (RMSE); along with the statistical method for model evaluation outlined by Willmott (1982), Willmott et al. (1985) and Willmott et al. (2012). This includes the separation of RMSE into its systematic ($RMSE_s$), and unsystematic ($RMSE_u$) components, and the Index of agreement. For this study the refined version of the Index of agreement (d_r) is used (Eq. 2 and Eq. 3), given that it includes improvements from the original version.

$$1 - \frac{\sum_{i=1}^{n}|\hat{y}_i - y_i|}{C\sum_{i=1}^{n}|y_i - \bar{y}|}, \text{ when} \quad (2)$$

$$\sum_{i=1}^{n}|\hat{y}_i - y_i| \leq C\sum_{i=1}^{n}|y_i - \bar{y}|, \text{ or}$$

$$\frac{C\sum_{i=1}^{n}|y_i - \bar{y}|}{\sum_{i=1}^{n}|\hat{y}_i - y_i|} - 1, \text{ when} \quad (3)$$

$$\sum_{i=1}^{n}|\hat{y}_i - y_i| > C\sum_{i=1}^{n}|y_i - \bar{y}|$$

where n is the number of observations of y, y_i is the i_{th} observation, $\bar{y}$ is the mean, $\hat{y}_i$ represents the modeled value and C is a constant, equal to 2. The improvements of this version include an index range that is double of the original (range from -1 to 1), which provides greater separation when comparing models that perform relatively well, and the use of absolute rather than squared differences, which makes the index less sensitive to outliers (Willmott et al., 2012). The better performing green roof model should have lower values of RMSE and higher $RMSE_u$ relative to $RMSE_s$; and a d_r value closer to 1 (Comer et al., 2000; Willmott et al., 2012).

https://doi.org/10.5194/egusphere-2026-981
Preprint. Discussion started: 16 March 2026

3. Results

3.1 Weather conditions

During the summer period (DOY 182–243), conditions show persistently high daytime mean incoming shortwave radiation and relatively stable daily mean incoming longwave radiation. Daily mean air and surface temperatures remain elevated throughout the period, with surface temperatures consistently exceeding air temperatures, and exhibiting a relatively wide daytime temperature range as indicated by the min–max envelopes. Specific humidity shows moderate variability, with lower daily mean values generally coinciding with warmer, clearer days. Daily mean wind speeds remain low to moderate and vary mainly from day-to-day, indicating variability driven by changing synoptic conditions. Precipitation occurs on a limited number of days, with most events near 10 mm (Fig. 3).

https://doi.org/10.5194/egusphere-2026-981
Preprint. Discussion started: 16 March 2026

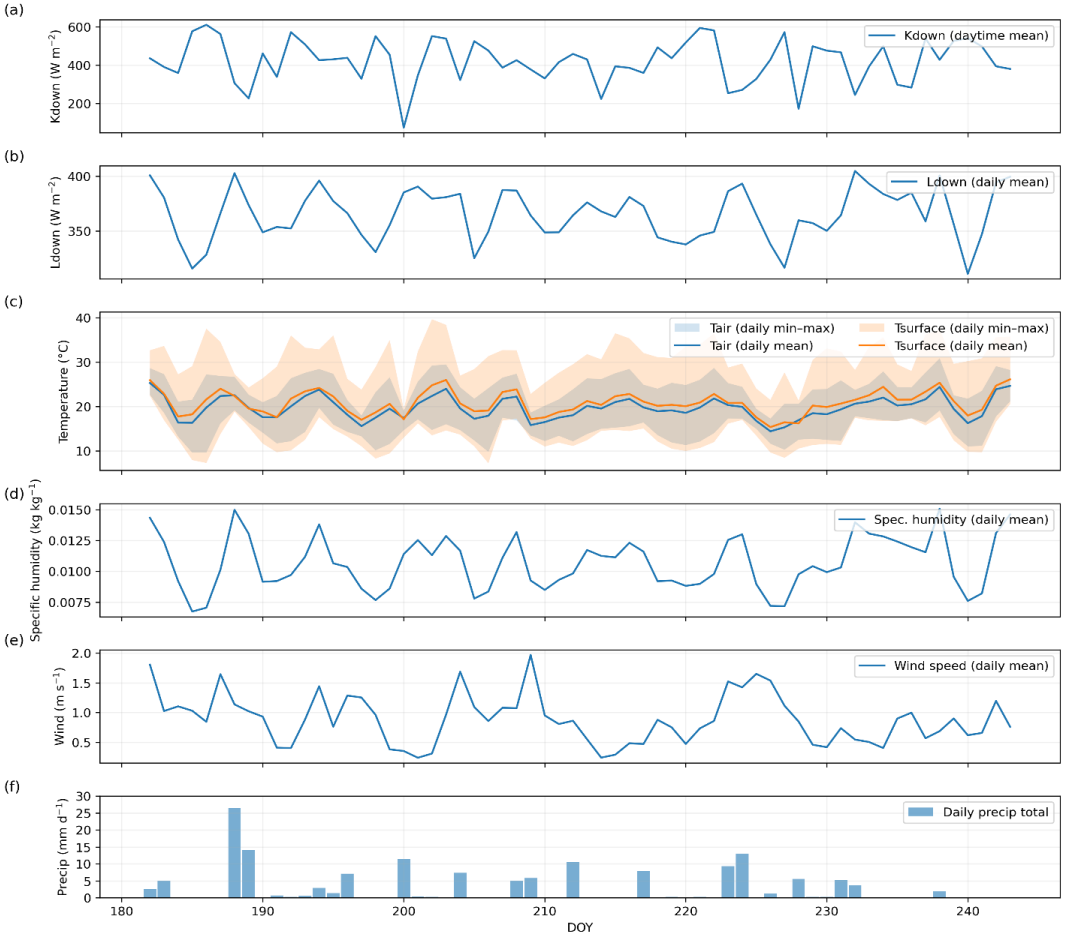

Figure 3: Weather conditions during the summer period. Panels a) and b) show daytime mean incoming shortwave (Kdown) and daily mean longwave (Ldown) radiation, respectively; panel c) shows daily mean air and surface temperatures with shaded envelopes indicating the daily minimum–maximum temperature range.; panel d) shows daily mean specific humidity; panel e) shows daily mean wind speed; and panel f) shows daily precipitation totals.

During the fall period (DOY 244–304), daytime mean incoming shortwave radiation decreases relative to summer and shows greater day-to-day variability, while daily mean incoming longwave radiation remains comparatively stable. Daily mean air and surface temperatures decline over the

https://doi.org/10.5194/egusphere-2026-981
Preprint. Discussion started: 16 March 2026

period, and the daily temperature range becomes narrower. Daily mean specific humidity is generally lower than during summer, consistent with cooler atmospheric conditions, while daily mean wind speeds show increased day-to-day variability. Precipitation occurs on a similar number of days as in summer, with most events below 10 mm and two significant larger rainfall events (Fig. 4).

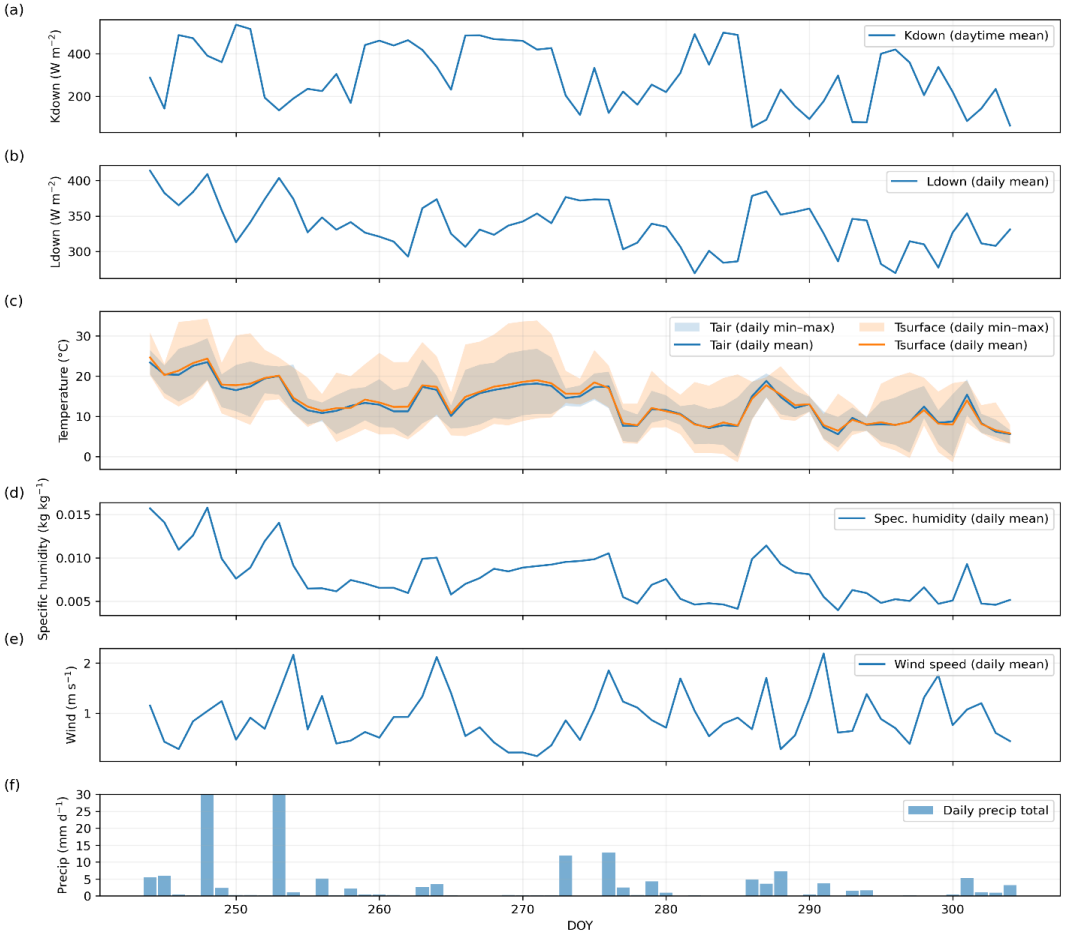

Figure 4: Weather conditions during the fall period. Panels a) and b) show daytime mean incoming shortwave (Kdown) and daily mean longwave (Ldown) radiation, respectively; panel c) shows daily mean air and surface temperatures with shaded envelopes indicating the daily minimum–maximum temperature range.; panel d) shows daily mean specific

https://doi.org/10.5194/egusphere-2026-981
Preprint. Discussion started: 16 March 2026

humidity; panel e) shows daily mean wind speed; and panel f) shows daily precipitation totals.

3.2 Observed energy balance

To characterize the surface energy exchange at the study site, we first examined the observed energy balance (Fig. 5). The hourly composites show a similar overall structure. In summer (Fig. 5a) mean Q^* peaks around ~450 W m^{-2} and is partitioned primarily into Q_h (50%), while Q_e accounts for 46% of daytime energy and Q_g for roughly 4%. T_{surf} peaks near ~30 °C. In fall (Fig. 5b), all components decrease seasonally: midday mean Q^* is ~300 W m^{-2}, Q_e represents 41% of the energy and Q_g contributes 7% of the energy. T_{surf} peaks around 20 °C.

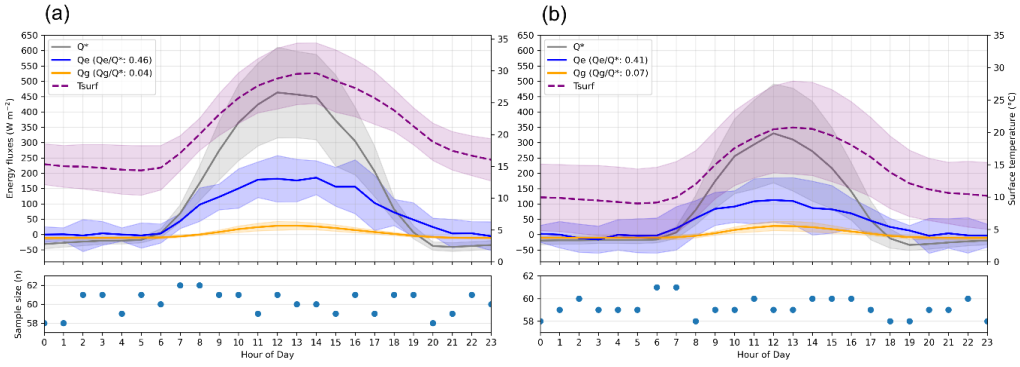

Figure 5: a) Hourly composite diurnal cycle of the observed energy balance components for the summer period (June-August), and b) the fall period (September-October), lower panels indicate the number of samples contributing to each hourly mean.

These composites illustrate how the green-roof energy balance evolves between periods, providing a reference framework for the subsequent model evaluation. Observed uncertainties were quantified using standard error propagation methods (Taylor, 1997), yielding mean daytime uncertainties of ±39 W m^{-2} for Q_e and ±14 W m^{-2} for Q_g. This helps contextualize the significance of the model–observation differences discussed below. Further details on the uncertainty propagation are provided in Sect. S3 and S4 of the supplementary materials.

https://doi.org/10.5194/egusphere-2026-981
Preprint. Discussion started: 16 March 2026

3.3 Comparative model evaluation

3.3.1 Latent heat flux

The hourly composites (Fig. 6) shows the two ER configurations (ER_o and ER_m) exhibiting early-morning underestimations and an afternoon positive bias, peaking around ~50 W m^{-2}. In contrast, WRF-MLGR consistently underestimates Q_e during the morning, and most of the afternoon, with biases reaching 100 W m^{-2}, later in the afternoon the model switches to overestimations. The shaded envelopes show larger variability for ER than for WRF-MLGR. In the summer period (Fig. 6a), ER_o shows stronger early-morning underestimations but smaller midday overestimation that ER_m, while WRF-MLGR maintains its predominantly negative bias, particularly in the morning. In the fall period (Fig. 6b) all models show reduced amplitudes, but the same general patterns persist: ER transitions from morning underestimation to afternoon overestimation and WRF-MLGR remains negatively biased.

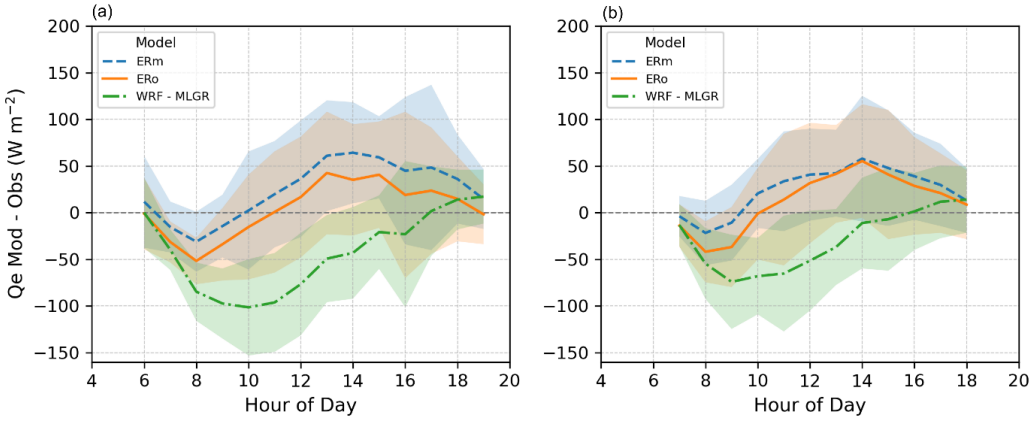

Figure 6: Hourly composite of the difference between modeled and observed Q_e for a) the summer period and b) the fall period.

Figure 7 presents the composite differences between modeled and observed Q_e—during daytime hours without active precipitation—, separated into dry days (< 0.2 mm of rainfall on the target day and during the preceding two days.; Fig. 7a) and rainy days (daily rainfall > 5 mm; Fig. 7b). On dry days, model behavior closely resembles that of the full-period composites and shows relatively small variability. In contrast, rainy days exhibit substantially larger variability across all models. The ER configurations retain the morning-to-afternoon bias reversal but with less

https://doi.org/10.5194/egusphere-2026-981
Preprint. Discussion started: 16 March 2026

consistent timing and a wider spread, whereas WRF-MLGR shows strong and persistent underestimation accompanied by a pronounced spread.

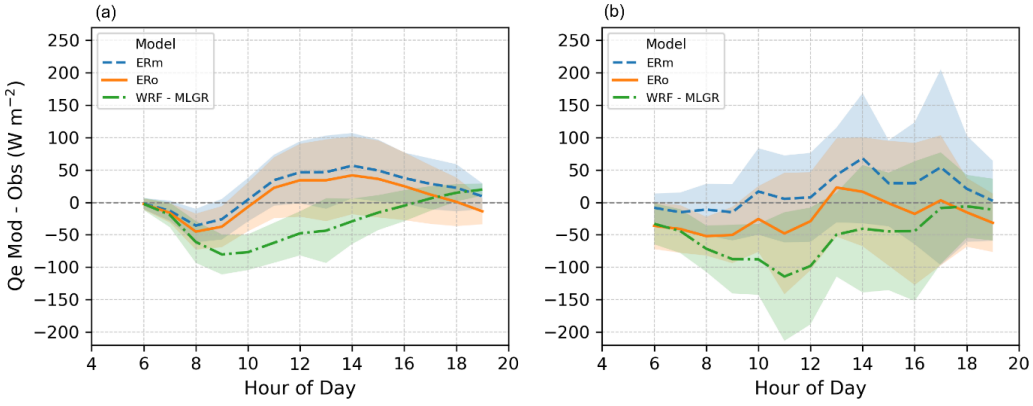

Figure 7: Hourly composite of the difference between modeled and observed Q_e for a) dry days and b) rainy days.

Days with high net radiation (Fig. 8a) reproduce the full-period diurnal pattern, with both ER configurations showing slightly larger mean differences, and all models exhibiting a relatively narrow spread. In contrast, low net radiation days (Fig. 8b) display a markedly different behavior, characterized by substantially increased variability and much smaller mean biases across all models.

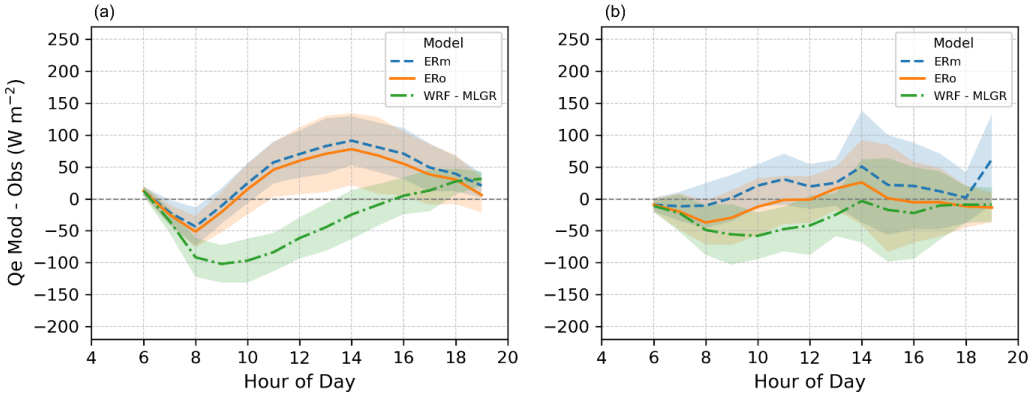

Figure 8: Hourly composite of the difference between modeled and observed Q_e for a) high net radiation days and b) low net radiation days.

https://doi.org/10.5194/egusphere-2026-981
Preprint. Discussion started: 16 March 2026

The statistical metrics (Table 2) are consistent with these patterns. ER shows slightly superior performance during the summer period: both ER versions retain positive MBE yet achieve marginally lower MAE than WRF-MLGR and higher d_r values (both ER_o and $ER_m \approx 0.60$ vs 0.50). For the fall season MAE and d_r are very similar between ER_o and WRF-MLGR, while ER_m shows slightly lower MAE and higher d_r. RMSE decomposition shows that ER errors are dominated by unsystematic errors. WRF-MLGR shows the opposite behavior, with systematic underestimation dominating.

Table 2: Statistical evaluation metrics for the Q_e for ER_o, ER_m, and WRF-MLGR models. Metrics include the Mean Absolute Error (MAE), Mean Bias Error (MBE), Root Mean Squared Error (RMSE), its unsystematic (RMSEu) and systematic (RMSEs) components, all in W m^{-2} and refined index of agreement (d_r).

	ER - original		*ER - modified*		*WRF-MLGR*	
	Summer	Fall	Summer	Fall	Summer	Fall
MAE	47.0	46.2	46.9	41.0	58.8	44.1
MBE	2.8	13.2	20.5	22.7	-48.8	-35.7
d_r	0.60	0.50	0.60	0.56	0.50	0.52
RMSE	60.7	60.0	59.3	53.0	77.6	61.6
RMSEu	60.5	58.2	55.4	47.8	47.4	38.6
RMSEs	4.6	14.5	21.2	22.8	61.4	48.0

3.3.2 Surface temperature

Both ER configurations show a persistent warm bias throughout the day, with the largest differences occurring in the afternoon. In contrast, WRF-MLGR shows a different pattern, characterized by morning underestimation followed by substantial afternoon overestimation. During the summer period both ER configurations maintain this warm bias and exhibit greater day-to-day variability than WRF-MLGR, particularly during the warmest hours. In the fall period, bias magnitudes are reduced for all models and variability decreases for ER, reflecting the overall weaker radiative forcing and more moderate surface temperatures (see Fig. S1 of supplementary materials).

Mean surface temperature biases are generally amplified under dry conditions and reduced on rainy days. This contrast is modest for the ER configurations, which maintain a similar warm bias across both moisture regimes, but is much more pronounced for WRF-MLGR. Under wetter

https://doi.org/10.5194/egusphere-2026-981
Preprint. Discussion started: 16 March 2026

conditions, bias magnitudes and diurnal range are dampened, and variability decreases (see Fig. S2 of supplementary materials).

High net radiation conditions (Fig. 9a) accentuate both diurnal temperature biases and variability. Under these conditions, ER exhibits increased daytime variability, while WRF-MLGR shows a comparatively narrower spread. Mean bias magnitudes remain comparable to those of the full evaluation periods, although morning underestimation in WRF-MLGR is slightly enhanced under strong radiative forcing. In contrast, low net-radiation conditions (Fig. 9b) are characterized by substantially reduced mean temperature differences for all models, most notably for WRF-MLGR. While variability in WRF-MLGR increases slightly under low net radiation conditions, the ER configurations show more stable behavior.

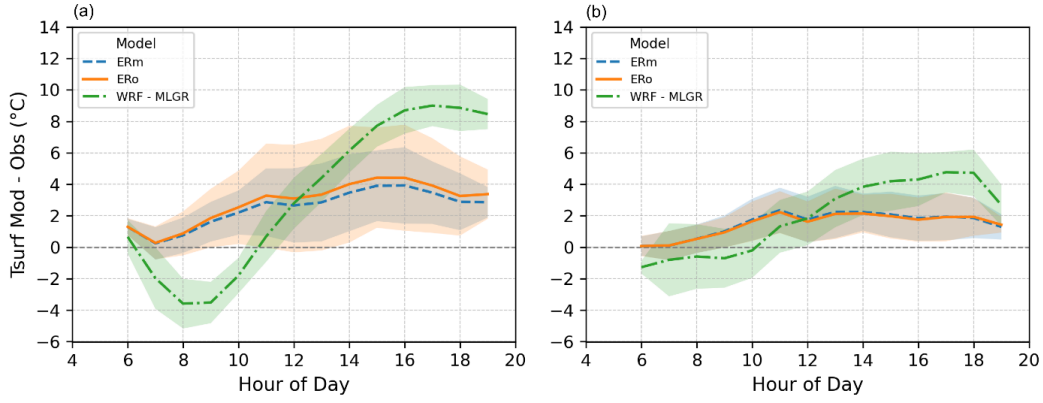

Figure 9: Hourly composite of the difference between modeled and observed T_{surf} for a) high net radiation days and b) low net radiation days.

Table 3 summarizes the statistical metrics for T_{surf} and reinforces the patterns seen in the diurnal composites. All models exhibit positive MBE, confirming T_{surf} warm biases. ER shows lower MAE values and higher d_r than WRF-MLGR in both periods, indicating smaller overall deviations from observations. The RMSE decomposition shows that ER's errors are dominated by their systematic component, consistent with the stable warm bias seen in the diurnal plots. WRF-MLGR, in contrast, exhibits a greater contribution from the unsystematic component. However, this statistical partitioning should not be interpreted as random variability. Rather, it reflects the consistent shift from morning underestimation to afternoon overestimation within the daytime period. These

https://doi.org/10.5194/egusphere-2026-981
Preprint. Discussion started: 16 March 2026

opposing biases partly offset each other in the MBE but remain large in magnitude, leading to elevated RMSE. Therefore, the large error components in WRF-MLGR indicate a structural timing and magnitude error in surface heating rather than random variability.

Table 3: Statistical evaluation metrics for T_{surf} for ER_o, ER_m, and WRF-MLGR models. Metrics include the Mean Absolute Error (MAE), Mean Bias Error (MBE), Root Mean Squared Error (RMSE), its unsystematic (RMSEu) and systematic (RMSEs) components, all in °C, and refined index of agreement (d_r).

	ER - original		*ER - modified*		*WRF-MLGR*	
	Summer	Fall	Summer	Fall	Summer	Fall
MAE	3.3	2.1	2.8	2.2	4.4	3.6
MBE	3.2	2.0	2.7	2.1	2.9	2.6
d_r	0.66	0.82	0.71	0.81	0.54	0.68
RMSE	4.4	2.6	3.6	2.7	5.4	4.6
RMSEu	2.9	1.5	2.3	1.6	4.2	3.7
RMSEs	3.3	2.1	2.8	2.2	3.3	2.7

3.3.3 Soil Heat Flux

Q_g exhibits the largest model–observation discrepancies for WRF-MLGR in both evaluation periods. Bias magnitudes are substantially larger than for the ER configurations, with peak overestimations exceeding 200 W m^{-2}, followed by a reversal to substantial underestimation in the late afternoon. In contrast, both ER configurations remain close to observations, with small consistently positive biases and low variability. Seasonal differences are modest: WRF-MLGR errors are larger in summer, while ER shows similarly stable behavior across both seasons, with reduced variability during fall (see Fig. S3 of supplementary materials).

Mean Q_g differences are generally reduced during rainy days relative to dry conditions. Under rainy conditions, the ER configurations remain close to zero throughout the day, while WRF-MLGR shows a marked reduction in bias magnitude but a substantially wider spread, indicating increased variability and less consistent timing (see Fig. S4 of supplementary materials).

High net-radiation conditions (Fig. 10a) strongly amplify Q_g biases, particularly for WRF-MLGR, which exhibits large midday overestimations that peak near ~250 W m^{-2} and a relatively narrow

https://doi.org/10.5194/egusphere-2026-981
Preprint. Discussion started: 16 March 2026

spread. In contrast, the ER configurations remain close to observations with limited variability. Under low net radiation conditions (Fig. 10b) the magnitude of Q_g biases decreases for all models. For WRF-MLGR, mean differences are substantially reduced, however, the spread widens substantially, reflecting increased day-to-day variability under weaker radiative forcing.

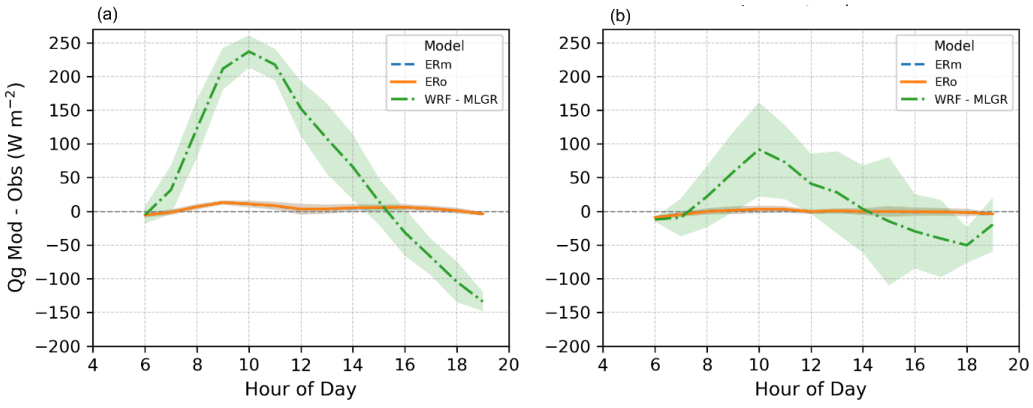

Figure 10: Hourly composite of the difference between modeled and observed Q_g for a) high net radiation days and b) low net radiation days.

Table 4 reinforces these contrasts. ER performs well, with both configurations showing nearly the same performance during both seasons, in the fall they show modest MAE values (~7 W m^{-2}), relatively high RMSE (~35 W m^{-2}) and high index of agreement (d_r = 0.77 for ER_o and 0.78 for ER_m). The summer period shows a small MAE for both configurations (~7 W m^{-2}) and relatively low RMSE (~9 W m^{-2}), these errors were dominated by the systematic component during the fall period, and by the unsystematic component during the summer period.

In contrast, WRF-MLGR performs very poorly, showing very large MAE (83 W m^{-2} for the fall and 103 W m^{-2} for the summer), RMSE (110 and 128 W m^{-2}), and strongly negative d_r values (−0.64 and -0.75), indicating poor temporal agreement. As observed for T_{surf}, the RMSE decomposition attributes a large portion of the error to the unsystematic component; however, the diurnal composites display a consistent phase pattern. The large error magnitudes in WRF-MLGR therefore reflect a systematic mismatch in the timing and magnitude of Q_g rather than random variability.

https://doi.org/10.5194/egusphere-2026-981
Preprint. Discussion started: 16 March 2026

Table 4: Statistical evaluation metrics for the Q_g for ER_o, ER_m, and WRF-MLGR models. Metrics include the Mean Absolute Error (MAE), Mean Bias Error (MBE), Root Mean Squared Error (RMSE), its unsystematic (RMSEu) and systematic (RMSEs) components all in W m^{-2}, and refined index of agreement (d_r).

	ER - original		*ER - modified*		*WRF-MLGR*	
	Summer	Fall	Summer	Fall	Summer	Fall
MAE	7.0	6.9	7.3	6.7	103.3	82.9
MBE	4.2	3.8	4.3	3.6	63.9	46.6
d_r	0.73	0.77	0.72	0.78	-0.75	-0.64
RMSE	8.7	34.6	8.9	34.6	127.6	109.5
RMSEu	7.3	16.2	7.4	15.9	97.6	99.0
RMSEs	4.7	30.6	5.0	30.8	82.3	46.9

3.3.4 Moisture content

Figure 11 shows the evolution of observed and modeled water content throughout summer (Fig. 11a) and fall (Fig. 11b). All models reproduce the timing of rainfall events, showing sharp increases in SWC after precipitation. However, the magnitude of these responses differs substantially across models.

During the summer period (Fig. 11a), ER_m shows the closest agreement with the observed peaks and subsequent dry-down trajectories. ER_o responds well to rainfall but generally produces larger peak values and drains more rapidly, leading to underestimation between events. WRF-MLGR consistently underpredicts SWC, with peak magnitudes consistently lower than observed and with faster post-rainfall declines.

In the fall period (Fig. 11b), the two ER configurations converge, producing very similar dynamics, with ER_o slightly closer to observations, particularly during the later part of the dry-downs. WRF-MLGR continues to reproduce the correct timing of wetting and drying but maintains well below observed magnitude.

https://doi.org/10.5194/egusphere-2026-981
Preprint. Discussion started: 16 March 2026

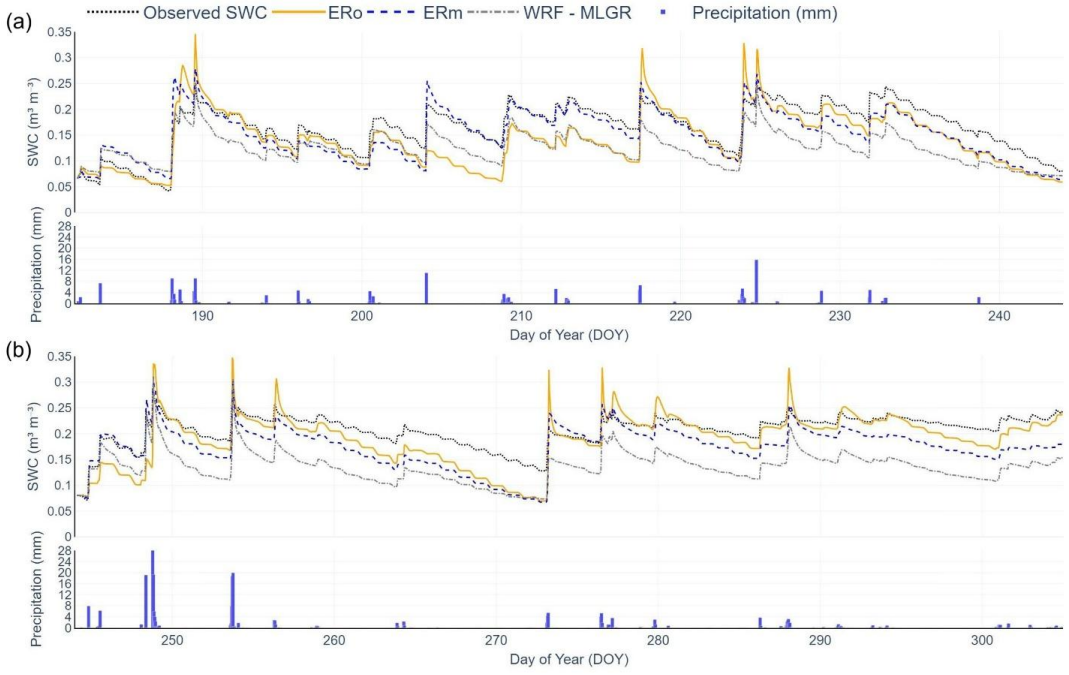

Figure 11: Time series of observed and modeled water content, with precipitation for a) the summer period and b) the fall period. Solid lines represent the model simulations (ER_o, ER_m, and WRF-MLGR), the dashed line shows the observations, and red bars indicate precipitation.

Table 5 highlights the contrast in model performance for water content. All models show negative MBE, confirming overall underestimation. The MAE values for the ER configurations are relatively small (0.030 $m^3 m^{-3}$ in the summer and 0.022 in the fall for ER_o; 0.021 $m^3 m^{-3}$ in the summer and 0.035 in the fall for ER_m), when compared with WRF-MLGR, which shows larger errors, with MAE reaching 0.045 $m^3 m^{-3}$ in the summer and 0.070 in the fall. Model agreement follows the same trend: ER achieves moderate d_r values, with the original configuration performing more consistently. In contrast, WRF-MLGR yields d_r values near zero (or negative), indicating poor agreement in magnitude despite reproducing event timing; its strong systematic dry bias (relatively large negative MBE) and damped storage response dominate the agreement score. RMSE values also favor ER (0.038 $m^3 m^{-3}$ and 0.029 for ER_o; 0.025 $m^3 m^{-3}$ and 0.039 for ER_m) over WRF-MLGR (0.048 and 0.073 $m^3 m^{-3}$). For ER_o, RMSE reflects a balance of systematic and unsystematic components, while ER_m shows larger unsystematic errors during summer but

https://doi.org/10.5194/egusphere-2026-981
Preprint. Discussion started: 16 March 2026

larger systematic errors in the fall. WRF-MLGR errors are dominated by systematic underestimation, consistent with its low storage representation.

Table 5: Statistical evaluation metrics for the moisture content for ER_o, ER_m, and WRF-MLGR models. Metrics include the Mean Absolute Error (MAE), Mean Bias Error (MBE), Root Mean Squared Error (RMSE), its unsystematic (RMSEu) and systematic (RMSEs) components all in $m^3\ m^{-3}$ and refined index of agreement (d_r).

	ER - original		*ER - modified*		*WRF-MLGR*	
	Summer	Fall	Summer	Fall	Summer	Fall
MAE	0.030	0.022	0.021	0.035	0.045	0.070
MBE	-0.024	-0.018	-0.012	-0.032	-0.039	-0.070
d_r	0.601	0.514	0.719	0.234	0.397	-0.356
RMSE	0.038	0.029	0.025	0.039	0.048	0.073
RMSEu	0.029	0.020	0.021	0.023	0.017	0.018
RMSEs	0.025	0.021	0.013	0.032	0.045	0.071

4. Discussion

4.1 Green roof observed energy balance

Relatively few studies report all surface energy balance components for green roofs simultaneously; however, many report individual components. As a result, reported observational energy balance values span a wide range, reflecting differences in climate, vegetation type, substrate moisture conditions, roof configuration, and measurement approach.

Q_e and/or evapotranspiration rate, is the most frequently evaluated component in the green-roof literature, given it plays an important role in the cooling potential and hydrology of green roofs. At our study site, Q_e represents approximately 46 % of the net radiation during the summer period and 41% during fall. These fractions correspond to a daily mean of 71 W m^{-2} for the summer, and 36 W m^{-2} in the fall. These values are comparable in magnitude to those reported by in other green roof studies. Marasco et al. (2015), for example, observed daily mean Q_e values of approximately 44–55 W m^{-2} for two full-scale extensive Sedum roofs in New York City, averaged over multiple years. Gößner et al. (2025) similarly reported daily mean evapotranspiration rates equivalent to a Q_e of approximately 49 W m^{-2} for ground-level extensive green roof systems in southern Germany, based on two years of observations. Despite differences in climate and experimental setup, the

https://doi.org/10.5194/egusphere-2026-981
Preprint. Discussion started: 16 March 2026

similarity in daily mean Q_e magnitudes across studies indicates that the observed fluxes at our site are consistent with those reported for green roofs elsewhere. The seasonal separation applied in the present study likely explains the higher summer and lower fall daily means relative to the multi-year averages reported in these studies. In contrast, other studies report higher Q_e for systems with denser vegetation or garden-style rooftops, such as the rooftop garden examined by Dong et al. (2025) where daily mean Q_e reached approximately 209 W m^{-2}.

Observational estimates of Q_g for green roof surfaces are less commonly reported. Heusinger & Weber (2017), who evaluated the surface energy balance of a full-scale extensive Sedum roof, reported a daytime mean Q_g values of 36 W m^{-2} during June-August and 19 W m^{-2} during September-November. In contrast, our measurements indicate lower daytime mean Q_g—12 W m^{-2} in the summer (July-August) and 13 W m^{-2} in the fall (September-October). This difference is likely related to the configuration of our green roof system, which is elevated above the rooftop surface, creating an air gap between the module and the roof deck that acts as an additional insulating layer.

To assess the influence of this configuration, one heat flux module (Fig. 2) was temporarily relocated to a location on the roof were it was in direct contact with the roof surface, and Q_g was then measured over a short period in October (Fig. 12). Under these conditions, the daytime mean Q_g increased to 23 W m^{-2}, better aligning with the September-November values reported by Heusinger & Weber (2017). Although this relocation experiment was conducted over a relatively short period in fall, the results suggest that the elevated configuration of our modules reduces conductive heat transfer. A longer evaluation period, particularly including summer conditions, would likely yield higher Q_g values, as suggested by the larger June–August means reported by Heusinger & Weber (2017).

https://doi.org/10.5194/egusphere-2026-981
Preprint. Discussion started: 16 March 2026

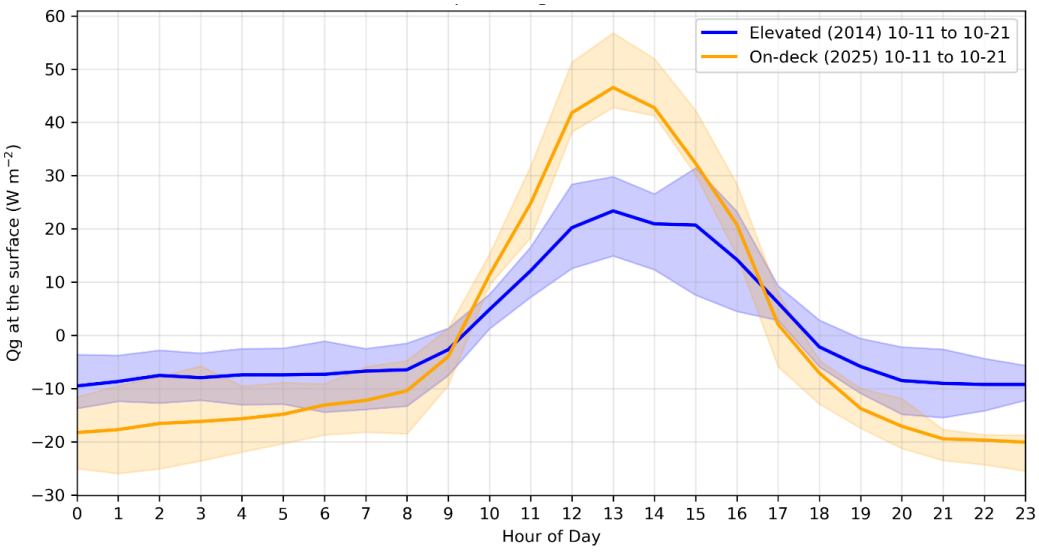

Figure 12: Hourly composite diurnal cycle of the observed soil heat flux (Q_g) for the elevated green roof on-deck configurations, data ranges from Oct. 11 to Oct 21 for both 2014 and 2025. Solid lines show the mean Q_g, while the shaded bands indicate ±1 standard deviation.

4.2 Physical behavior of the models

Because the two ER configurations (ER_o and ER_m) produced very similar results, the discussion focuses on the general physical behavior of the ER model rather than on version-specific differences. The refinements introduced in the modified version did not fundamentally alter the model's energy-partitioning behavior. As a result, the dominant contrasts in model performance arise not between the ER versions but between ER and WRF-MLGR, which differ structurally in vegetation representation, stomatal and aerodynamic resistance formulations, and soil hydrology. Thus, the discussion refers to "ER" generically when examining the physical basis of model behavior.

4.2.1 Latent heat flux

ER consistently overestimated Q_e, whereas WRF-MLGR produced negative deviations. The ER bias can be traced to the model's simplified representation of vegetation controls on transpiration. Because ER computes latent heat flux as the sum of soil evaporation, transpiration—and evaporation of intercepted water, in the case of ER_m—transpiration dominates under vegetated

https://doi.org/10.5194/egusphere-2026-981
Preprint. Discussion started: 16 March 2026

conditions and is strongly scaled by LAI. The relatively high LAI observed led ER to treat Sedum as fully active, despite the fact that CAM species typically maintain low transpiration rates through conservative stomatal regulation even under favorable environmental conditions (Gravatt and Martin, 1992; Huang et al., 2024).

The ER model's stomatal resistance formulation does not capture this conservative behavior. In ER, minimum stomatal resistance is adjusted only by radiation-, moisture-, and VPD-based stress functions, which allows stomata to remain relatively open until VPD becomes high. CAM plants, however, exhibit earlier stomatal closure, responding directly to atmospheric demand through a "feed-forward" mechanism that is not represented in the model (Males & Griffiths; 2017). As a result, ER overestimates transpiration during conditions under which Sedum would physiologically restrict water loss.

WRF-MLGR represents latent heat flux solely through transpiration, as the current version does not include a soil evaporation term. This structural limitation causes systematic underestimation of Q_e. In addition, WRF-MLGR places greater emphasis on aerodynamic resistance and applies strong atmospheric controls on stomatal resistance, including air temperature. While this yields behavior more consistent with the conservative water-use strategy of CAM vegetation, it can also amplify the underestimations by suppressing transpiration prematurely under rising temperature and VPD, reinforcing the negative biases seen in the statistical evaluation. Thus, although WRF-MLGR represents Sedum's conservative stomatal behavior more realistically than ER, the absence of a soil evaporation component and the strong atmospheric regulation of stomatal resistance contribute to underestimations over the diurnal cycle.

4.2.2 Surface temperature and soil heat flux

Both models overestimate daytime T_{surf} and Q_g, though for different reasons and with different magnitudes. ER shows a modest but systematic warm bias (≈1–3 °C), possibly because the model lacks vegetation heat capacity and therefore cannot buffer short-term fluctuations in net radiation. Combined with small energy misallocations among Q_e, Q_h, and Q_g, this causes excess energy to accumulate at the surface, producing a consistent warm bias despite the model's tendency to overestimate latent heat flux. Correspondingly, ER produces small but systematic overestimations of Q_g, which primarily stem from biases in the near-surface temperature gradient. Although the

https://doi.org/10.5194/egusphere-2026-981
Preprint. Discussion started: 16 March 2026

model includes a moisture-dependent conductivity formulation, this representation does not fully capture the observed variation in k for the studied substrate (Perelli, 2014). Nevertheless, retaining the original formulation results in realistic Q_g magnitudes because the smaller conductivity partially offsets the warm bias in the simulated surface and shallow soil temperatures. As a result, the residual errors in Q_g remain modest and consistent throughout the day, as reflected in the small RMSE values and the relatively flat diurnal difference curves for both ER versions.

In contrast, WRF-MLGR exhibits a much larger positive bias in T_{surf}, particularly during the afternoon, along with very large Q_g errors, and failure to reproduce the observed Q_g diurnal cycle. The most likely reason for this bias is the lack of vegetation radiative representation, meaning all shortwave and longwave radiation is absorbed at the "combined soil-vegetation" surface, with effectively no shading of the soil surface, canopy heat storage, or radiative interactions to moderate surface warming. As a result, incoming radiation is applied directly to the soil rather than to the vegetation that shades the substrate. Because soil has a much higher thermal admittance than foliage, a large fraction of the radiative forcing is initially stored as ground heat, leading to elevated morning values of Q_g as the energy accumulates in the upper soil layers. This stored energy governs the subsequent evolution of T_{surf} and delays the development of Q_h and Q_e, causing Q_g to dominate the diurnal partitioning of surface fluxes. This behavior contrasts with real vegetated surfaces, where the vegetation enables rapid adjustment of sensible and latent heat fluxes under increasing radiative forcing (Curtis, 1936; Tadeu et al., 2021). As part of the experimental green roof system tests, an unvegetated module was also instrumented and installed to monitor Q_g. Figure 13 illustrates how, as a consequence of this soil-dominated energy storage, the modeled Q_g presents a diurnal pattern that is more consistent with that of a bare substrate than with observations from the vegetated module.

https://doi.org/10.5194/egusphere-2026-981
Preprint. Discussion started: 16 March 2026

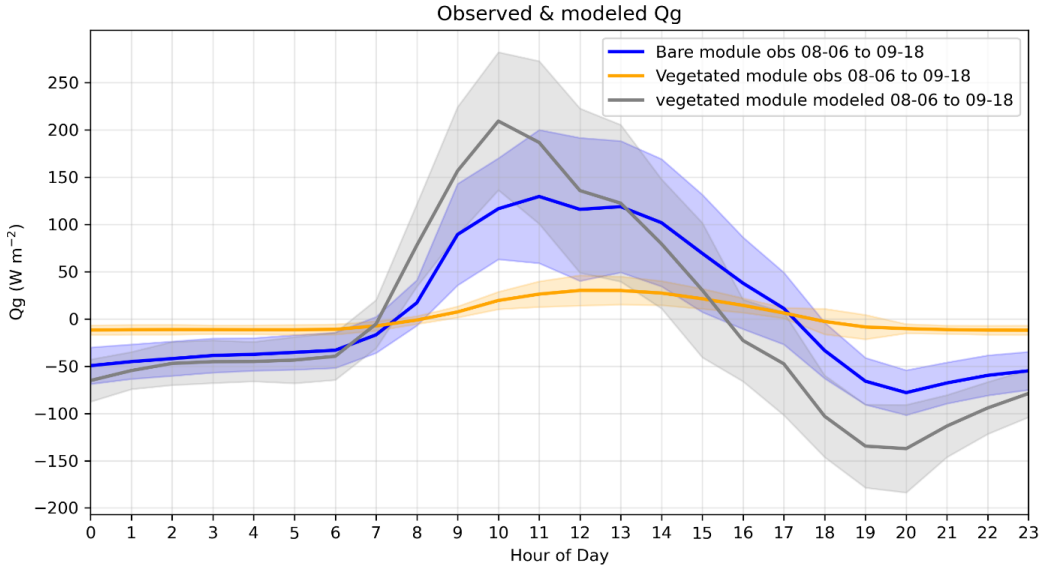

Figure 13: Hourly composite of the observed bare (non-vegetated) module (blue), observed vegetated module (yellow) and modeled vegetated module from WRF-MLGR (green) Q_g. Solid lines represent the mean value and the shaded areas represent ±1 standard deviation. Legend also includes the plotted dates.

4.2.3 Moisture Content

ER_o captures the timing of rainfall inputs but often produces larger post-rain increases in water content and a faster early decline than observed. This reflects the model structure in which precipitation is applied directly to the surface layer, producing an immediate increase in SWC in the upper layer. These peaks are followed by a rapid initial decline driven as internal redistribution transfers water from the surface layer to the subsurface layer, where it becomes available for gravitational drainage and transpiration. Redistribution also contributes directly to an early decrease in the depth-averaged water content by relaxing the unrealistically high surface-layer moisture. Although evapotranspiration is overestimated by the model, the early post-rain decrease is dominated by redistribution and drainage rather than an immediate enhancement of Q_e. Once soil moisture decreases, modeled and observed drying rates become more similar, however ER_o

https://doi.org/10.5194/egusphere-2026-981
Preprint. Discussion started: 16 March 2026

remains persistently drier because early post-rain redistribution and drainage reduce stored water more rapidly than in the observed system.

ER_m alters the water balance primarily through canopy interception and a moisture-dependent runoff formulation. A fraction of rainfall is temporarily stored on the foliage and evaporated directly, so only the remaining drip reaches the soil. This dampens the sharp post-rain increases in soil water content seen in ER_o and, for many events, brings the modeled peaks closer to observations. The new runoff parameterization also removes water from the surface layer as a function of saturation, providing an explicit drainage pathway when the soil is wet. Together, these changes reduce the magnitude of storage peaks and promote faster loss of excess water, so ER_m tracks the observed dry-down more closely but often remains slightly drier than ER_o between rainfall events.

In WRF-MLGR, the soil hydraulic parameters and free-drain bottom boundary allow water to percolate out of the soil column very efficiently when the profile is wet. Hydraulic conductivity in the deeper soil exhibits a strong nonlinear dependence on soil moisture, and the multilayer diffusion scheme rapidly transfers infiltrated water downward toward this drainage sink. As a result, the deeper layers tend to dry quickly following precipitation. Because these lower layers represent a substantial fraction of the total soil depth and the simulated bulk water content is computed as a depth-weighted average across all layers, their rapid drying strongly influences the overall column moisture. Consequently, the model exhibits a persistent dry bias relative to the lysimeter-derived bulk water content.

4.3 Model performance under different moisture regimes and radiative forcing conditions

4.3.1 Influence of moisture regime

Model performance exhibits a clear sensitivity to moisture regime across all evaluated variables. Under dry conditions, model behavior is generally more stable, with limited variability in all variables and more consistent biases in T_{surf} and Q_g. These conditions correspond to a moisture-limited regime in which surface energy partitioning is more predictable. In contrast, during the dry daytime hours of rainy days, mean differences are reduced, but variability in Q_e and Q_g and T_{surf} increase. This indicates that elevated substrate moisture and residual surface wetness increase the

https://doi.org/10.5194/egusphere-2026-981
Preprint. Discussion started: 16 March 2026

complexity of surface–atmosphere exchanges and introduce greater uncertainty in modeled fluxes and temperatures.

4.3.2 Influence of radiative forcing

Separating days by net radiation shows that radiative forcing primarily scales existing model biases rather than altering their structure. Under high net radiation, biases in Q_e, T_{surf} and Q_g are amplified, as greater available energy intensifies the expression of errors associated with each model's representation of vegetation and soil processes, leading to more consistent error patterns. Under low net radiation, error magnitudes are reduced but become more variable, as limited energy availability constrains fluxes and increases sensitivity to day-to-day atmospheric variability. These results indicate that radiative forcing does not introduce new sources of error but instead governs how strongly underlying model assumptions are expressed.

4.4 Implications for modeling and research

The findings of this study suggest that past applications of ER and WRF-MLGR should be interpreted with some caution. For ER, the systematic overestimation of Q_e implies that earlier studies may have overstated the evaporative cooling potential of green roofs, especially under high radiation and low moisture availability. Nevertheless, ER performed comparatively well in simulating Q_g and T_{surf}, indicating that it may be more reliable for studies focused on subsurface thermal dynamics or building-energy performance.

In contrast, WRF-MLGR exhibits structural limitations across all major components of the surface energy balance. Although the model shows an overall moderate agreement for Q_e, the lack of a soil-evaporation term, means Q_e is represented solely through transpiration, leading to persistent underestimations. The absence of an explicit vegetation canopy also allows incoming radiation to interact directly with the soil, increasing the radiative load on this (relatively) high thermal admittance surface (instead of the low thermal admittance vegetation) and amplifying surface heat storage and release. T_{surf}, which is tightly coupled to Q_g, consequently exhibits pronounced daytime warm biases. Taken together, these highlight areas where WRF-MLGR would benefit from further refinement to improve its suitability for green roof applications. Our team has further developed

https://doi.org/10.5194/egusphere-2026-981
Preprint. Discussion started: 16 March 2026

this model to address these main limitations and its performance against observations is much improved, particularly for Q_g (Saeedi et al., 2026).

More broadly, this study underscores the importance of rigorous, process-level evaluation in modeling of green roofs and of urban heat adaptation strategies more generally (Krayenhoff et al. 2021). Users of ER or WRF-MLGR should be aware of each model's structural assumptions and characteristic biases and should evaluate outputs against local green roof energy balance observations whenever possible. Accurate representation of the surface energy balance is essential for credible assessments of green roof performance. Ultimately, selecting an appropriate model—and clearly acknowledging its limitations—will be key to producing robust, policy-relevant assessments of green roof performance in urban environments.

5. Conclusion

This research presented a detailed evaluation of two green roof energy balance models—EcoRoof (EnergyPlus) and WRF-MLGR—using observational data collected from a *Sedum*-covered green roof test array. By comparing simulated and observed values of Q_e, Q_g, and T_{surf} across multiple environmental conditions, this study provided insights into model behavior, limitations, and applicability. The results revealed that both models exhibit biases, though for different reasons rooted in their structure and assumptions. EcoRoof consistently and modestly overestimated Q_e and T_{surf}, partly due to vegetation parameter sensitivity and simplified representations of surface–atmosphere exchanges. In contrast, WRF-MLGR underestimated Q_e, and strongly overestimated T_{surf} and Q_g, likely due to its lack of an explicit vegetation layer and consequent primary site of radiation exchange being a hybrid "soil-vegetation" layer with substantial thermal admittance.

Beyond reporting performance metrics, this study highlights the importance of comprehensive, process-level model evaluation—an aspect often lacking in prior green roof modeling studies—and underscores the need for future model developments that ensure physically consistent flux formulations. In particular, vegetation-specific physiology, canopy and substrate heat storage, radiative absorption, and the distinct evaporation and transpiration pathways. These findings are particularly relevant for the integration of green roof schemes into urban canopy and building

https://doi.org/10.5194/egusphere-2026-981
Preprint. Discussion started: 16 March 2026

energy models, where accurate representation of surface energy partitioning is critical for assessing heat mitigation potential and informing strategies to improve urban climate resilience.

Code and data availability. The exact stand-alone versions of the green roof model configurations used to produce the results presented in this study are archived in a persistent public repository at Zenodo: https://doi.org/10.5281/zenodo.18688590 (Martinez Mendoza et al., 2026). The archived release corresponds to the precise versions of the codes, input forcing data, observational datasets and post processing scripts used in this research, ensuring reproducibility of the results.

The stand-alone WRF-MLGR implementations are derived from the WRF source code and are distributed under the GNU General Public License v2.0 or later (GPL v2+). The stand-alone EcoRoof implementations (original configuration ER_o and modified configuration ER_m), derived from EnergyPlus, are distributed under the BSD 3-Clause License. The observational datasets and post-processing scripts are distributed under the Creative Commons Attribution 4.0 International (CC BY 4.0) license.

The ER model is based on the green roof module originally described by Sailor (2008) and implemented within EnergyPlus; the modified ER configuration follows the developments described by Heusinger (2018) and the WRF-MLGR green roof parameterization is based on the scheme described by Zonato et al. (2021). The observed data used for the evaluation were collected as part of a long-term field experiment conducted at Western University, London, ON, Canada.

Author contribution. MMM designed and implemented the evaluation methodology, performed all simulations, conducted all analyses, interpreted results and prepared the manuscript. AS extracted and implemented the green roof models, adapting components originally embedded within larger modeling frameworks. JAV supervised the work, assisted with the interpretation of results, suggested additional analyses, and reviewed and edited the manuscript. ESK contributed to the acquisition and implementation of the model codes, assisted with the interpretation of results, and reviewed and edited the manuscript.

Competing interests. The authors declare that they have no conflict of interest.

https://doi.org/10.5194/egusphere-2026-981
Preprint. Discussion started: 16 March 2026

Acknowledgements. We gratefully acknowledge Sylvie Leroyer for her guidance in the selection of the models; Dimuth Kurukulaarachchi for his extensive work on the green roof; and the 2014 green roof research team, led by Dennis O'Carroll, for collecting the observational data used in this study.

Financial support. This research was funded by the Climate Action and Awareness Fund, administered by Environment and Climate Change Canada.

References

Berardi, U.: The outdoor microclimate benefits and energy saving resulting from green roofs retrofits, Energy and Buildings, 121, 217–229, https://doi.org/10.1016/j.enbuild.2016.03.021, 2016.

Berardi, U., GhaffarianHoseini, A., and GhaffarianHoseini, A.: State-of-the-art analysis of the environmental benefits of green roofs, Applied Energy, 115, 411–428, https://doi.org/10.1016/j.apenergy.2013.10.047, 2014.

Cascone, S., Catania, F., Gagliano, A., and Sciuto, G.: A comprehensive study on green roof performance for retrofitting existing buildings, Building and Environment, 136, 227–239, https://doi.org/10.1016/j.buildenv.2018.03.052, 2018.

Comer, N. T., Lafleur, P. M., Roulet, N. T., Letts, M. G., Skarupa, M., and Verseghy, D.: A test of the Canadian land surface scheme (class) for a variety of wetland types, Atmosphere-Ocean, 38, 161–179, https://doi.org/10.1080/07055900.2000.9649644, 2000.

Costanzo, V., Evola, G., and Marletta, L.: Energy savings in buildings or UHI mitigation? Comparison between green roofs and cool roofs, Energy and Buildings, 114, 247–255, https://doi.org/10.1016/j.enbuild.2015.04.053, 2016.

Curtis, O. F.: LEAF TEMPERATURES AND THE COOLING OF LEAVES BY RADIATION, Plant Physiol., 11, 343–364, https://doi.org/10.1104/pp.11.2.343, 1936.

Dong, X., Feng, X., and He, B.-J.: Dual potential of Garden Rooftop Farms for heat island mitigation and spatial productivity, Building and Environment, 274, 112768, https://doi.org/10.1016/j.buildenv.2025.112768, 2025.

Gößner, D., Kunle, M., and Mohri, M.: Green roof performance monitoring: Insights on physical properties of 4 extensive green roof types after 2 years of microclimatic measurements, Building and Environment, 269, 112356, https://doi.org/10.1016/j.buildenv.2024.112356, 2025.

https://doi.org/10.5194/egusphere-2026-981
Preprint. Discussion started: 16 March 2026

672 Gravatt, D. A. and Martin, C. E.: Comparative ecophysiology of five species of Sedum
673 (Crassulaceae) under well-watered and drought-stressed conditions, Oecologia, 92, 532–541,
674 https://doi.org/10.1007/bf00317845, 1992.

675 He, Y., Yu, H., Ozaki, A., and Dong, N.: Thermal and energy performance of green roof and cool
676 roof: A comparison study in Shanghai area, Journal of Cleaner Production, 267, 122205,
677 https://doi.org/10.1016/j.jclepro.2020.122205, 2020.

678 Heusinger, J. and Weber, S.: Surface energy balance of an extensive green roof as quantified by
679 full year eddy-covariance measurements, Science of The Total Environment, 577, 220–230,
680 https://doi.org/10.1016/j.scitotenv.2016.10.168, 2017.

681 Heusinger, J., Sailor, D. J., and Weber, S.: Modeling the reduction of urban excess heat by green
682 roofs with respect to different irrigation scenarios, Building and Environment, 131, 174–183,
683 https://doi.org/10.1016/j.buildenv.2018.01.003, 2018.

684 Huang, J., Kong, F., Yin, H., Middel, A., Green, J. K., and Liu, H.: Green roof plant physiological
685 water demand for transpiration under extreme heat, Urban Forestry & Urban Greening, 98,
686 128411, https://doi.org/10.1016/j.ufug.2024.128411, 2024.

687 Imran, H. M., Kala, J., Ng, A. W. M., and Muthukumaran, S.: Effectiveness of green and cool
688 roofs in mitigating urban heat island effects during a heatwave event in the city of Melbourne in
689 southeast Australia, Journal of Cleaner Production, 197, 393–405,
690 https://doi.org/10.1016/j.jclepro.2018.06.179, 2018.

691 Jaffal, I., Ouldboukhitine, S.-E., and Belarbi, R.: A comprehensive study of the impact of green
692 roofs on building energy performance, Renewable Energy, 43, 157–164,
693 https://doi.org/10.1016/j.renene.2011.12.004, 2012.

694 Kalogeri, C., Spyrou, C., Koukoula, M., Saviolakis, P. M., Pappa, A., Loupis, M., Masouras, C.,
695 and Katsafados, P.: Modeling the Impact of the Green Roofs as a Nature-Based Solution to
696 Mitigate the Urban Heat Island Effects over Attica, Greece, in: 16th International Conference on
697 Meteorology, Climatology and Atmospheric Physics—COMECAP 2023, International
698 Conference on Meteorology, Climatology and Atmospheric Physics, Basel Switzerland, 174,
699 https://doi.org/10.3390/environsciproc2023026174, 2023.

700 Karachaliou, P., Santamouris, M., and Pangalou, H.: Experimental and numerical analysis of the
701 energy performance of a large scale intensive green roof system installed on an office building in
702 Athens, Energy and Buildings, 114, 256–264, https://doi.org/10.1016/j.enbuild.2015.04.055,
703 2016.

704 Khan, A., Khorat, S., Doan, Q., Khatun, R., Das, D., Hamdi, R., Carlosena, L., Santamouris, M.,
705 Georgescu, M., and Niyogi, D.: Exploring the Meteorological Impacts of Surface and Rooftop
706 Heat Mitigation Strategies Over a Tropical City, JGR Atmospheres, 128,
707 https://doi.org/10.1029/2022jd038099, 2023.

https://doi.org/10.5194/egusphere-2026-981
Preprint. Discussion started: 16 March 2026

Kim, S. H., Park, C. Y., Choi, J. Y., and Park, C.: Exploring maladaptive patterns of small-scale green roofs through evaluation in a capacity of heat mitigation: A case study in seoul, Building and Environment, 266, 112052, https://doi.org/10.1016/j.buildenv.2024.112052, 2024.

Krayenhoff, E. S., Martilli, A., Bass, B., and Stull, R. B.: Mesoscale simulation of urban heat mitigation strategies in Toronto, Canada, Fifth Int. Conf. on Urban Climate, 2003.

Krayenhoff, E. S., Broadbent, A. M., Zhao, L., Georgescu, M., Middel, A., Voogt, J. A., Martilli, A., Sailor, D. J., and Erell, E.: Cooling hot cities: a systematic and critical review of the numerical modelling literature, Environ. Res. Lett., 16, 053007, https://doi.org/10.1088/1748-9326/abdcf1, 2021.

Kurukulaarachchi, D. C.: Temporal Variability In The Daytime Green Roof Energy Balance During Drying Periods, MSc Thesis. The University of Western Ontario, 2017.

Li, D., Bou-Zeid, E., and Oppenheimer, M.: The effectiveness of cool and green roofs as urban heat island mitigation strategies, Environ. Res. Lett., 9, 055002, https://doi.org/10.1088/1748-9326/9/5/055002, 2014.

Liu, K. and Minor, J.: Performance Evaluation of an Extensive Green Roof, National Research Council Canada, 2005.

Males, J. and Griffiths, H.: Stomatal Biology of CAM Plants, Plant Physiol., 174, 550–560, https://doi.org/10.1104/pp.17.00114, 2017.

Marasco, D. E., Culligan, P. J., and McGillis, W. R.: Evaluation of common evapotranspiration models based on measurements from two extensive green roofs in New York City, Ecological Engineering, 84, 451–462, https://doi.org/10.1016/j.ecoleng.2015.09.001, 2015.

Martens, R., Bass, B., and Alcazar, S. S.: Roof–envelope ratio impact on green roof energy performance, Urban Ecosyst, 11, 399–408, https://doi.org/10.1007/s11252-008-0053-z, 2008.

Martilli, A., Clappier, A., and Rotach, M. W.: An Urban Surface Exchange Parameterisation for Mesoscale Models, Boundary-Layer Meteorology, 104, 261–304, https://doi.org/10.1023/A:1016099921195, 2002.

Martinez Mendoza, M., Saeedi, A., Voogt, J. A., and Krayenhoff, E. S.: Stand-alone EcoRoof (ERo, ERm) and WRF-MLGR model codes and evaluation datasets for "Process-based evaluation of green roof models for assessment of heat mitigation efficacy in WRF (v4.3.1) and EnergyPlus (v8.6.0)", Zenodo [code and data set], https://doi.org/10.5281/zenodo.18688590, 2026.

Oberndorfer, E., Lundholm, J., Bass, B., Coffman, R. R., Doshi, H., Dunnett, N., Gaffin, S., Köhler, M., Liu, K. K. Y., and Rowe, B.: Green Roofs as Urban Ecosystems: Ecological Structures, Functions, and Services, BioScience, 57, 823–833, https://doi.org/10.1641/B571005, 2007.

Perelli, G. A.: Characterization of the Green Roof Growth Media, MSc Thesis. The University of Western Ontario, 2014.

https://doi.org/10.5194/egusphere-2026-981
Preprint. Discussion started: 16 March 2026

743 Saeedi, A., Martinez Mendoza, M., Krayenhoff, E. S., Voogt, J., Zonato, A., Leroyer, S., and
744 Wagner-Riddle, C.: Process-based upgrades to the WRF multi-layer green-roof scheme (WRF-
745 MLGR v2.0) and evaluation against field observations, Geosci. Model Dev., in review, 2026.

746 Sailor, D. J.: A green roof model for building energy simulation programs, Energy and Buildings,
747 40, 1466–1478, https://doi.org/10.1016/j.enbuild.2008.02.001, 2008.

748 Salamanca, F., Krpo, A., Martilli, A., and Clappier, A.: A new building energy model coupled
749 with an urban canopy parameterization for urban climate simulations—part I. formulation,
750 verification, and sensitivity analysis of the model, Theor Appl Climatol, 99, 331–344,
751 https://doi.org/10.1007/s00704-009-0142-9, 2010.

752 Seo, Y., Kwon, Y., Hwang, J. S., and Woo, D. K.: A Comparative Experimental Study of Green
753 Roofs Based on Radiation Budget and Surface Energy Balance, KSCE J Civ Eng, 27, 1866–1880,
754 https://doi.org/10.1007/s12205-023-1491-0, 2023.

755 Shafique, M., Kim, R., and Rafiq, M.: Green roof benefits, opportunities and challenges – A
756 review, Renewable and Sustainable Energy Reviews, 90, 757–773,
757 https://doi.org/10.1016/j.rser.2018.04.006, 2018.

758 Siddiqui, K., et al.: Improved multi-scale GHG emissions modeling from urban environments to
759 enhance mitigation strategies, Environment and Climate Change Canada, Advancing Climate
760 Change Science and Technology 2021/2022, project description (2022–2026), 2022.

761 Silva, C. M., Gomes, M. G., and Silva, M.: Green roofs energy performance in Mediterranean
762 climate, Energy and Buildings, 116, 318–325, https://doi.org/10.1016/j.enbuild.2016.01.012,
763 2016.

764 Sun, T., Grimmond, C. S. B., and Ni, G.: How do green roofs mitigate urban thermal stress under
765 heat waves?, JGR Atmospheres, 121, 5320–5335, https://doi.org/10.1002/2016jd024873, 2016.

766 Tadeu, A., Škerget, L., Almeida, J., and Simões, N.: Canopy contribution to the energy balance of
767 a building's roof, Energy and Buildings, 244, 111000,
768 https://doi.org/10.1016/j.enbuild.2021.111000, 2021.

769 Taylor: An Introduction to Error Analysis. The Study of Uncertainties in Physical Measurements.,
770 Second., University Science Books, California, 1997.

771 Willmott, C., Ackleso, S., Davis, O., Feddema, J., Klink, K., Legate, D., and Rowe, A.: Statistics
772 for the Evaluation and Comparison of Models, Journal of Geophysical Research, 90, 8995–9005,
773 1985.

774 Willmott, C. J.: Some Comments on the Evaluation of Model Performance, Bull. Amer. Meteor.
775 Soc., 63, 1309–1313, https://doi.org/10.1175/1520-0477(1982)063<1309:SCOTEO>2.0.CO;2,
776 1982.

https://doi.org/10.5194/egusphere-2026-981
Preprint. Discussion started: 16 March 2026

777 Willmott, C. J., Robeson, S. M., and Matsuura, K.: A refined index of model performance, Intl
778 Journal of Climatology, 32, 2088–2094, https://doi.org/10.1002/joc.2419, 2012.

779 Zheng, X., Yang, Z., Yang, J., Tang, M., and Feng, C.: An experimental study on the thermal and
780 energy performance of self-sustaining green roofs under severe drought conditions in summer,
781 Energy and Buildings, 261, 111953, https://doi.org/10.1016/j.enbuild.2022.111953, 2022.

782 Zheng, Y. and Weng, Q.: Modeling the Effect of Green Roof Systems and Photovoltaic Panels for
783 Building Energy Savings to Mitigate Climate Change, Remote Sensing, 12, 2402,
784 https://doi.org/10.3390/rs12152402, 2020.

785 Zonato, A., Martilli, A., Gutierrez, E., Chen, F., He, C., Barlage, M., Zardi, D., and Giovannini,
786 L.: Exploring the Effects of Rooftop Mitigation Strategies on Urban Temperatures and Energy
787 Consumption, JGR Atmospheres, 126, e2021JD035002, https://doi.org/10.1029/2021JD035002,
788 2021.
789